Protein Kinase A is a Dependent Factor and Therapeutic Target in Fibrous Dysplasia

Contents	Page
Supplementary Figure 1	2
Supplementary Figure 2	3
Supplementary Figure 3	4
Supplementary Figure 4	5
Supplementary Figure 5	6
Supplementary Figure 6	7

SUPPLEMENTARY FIGURES

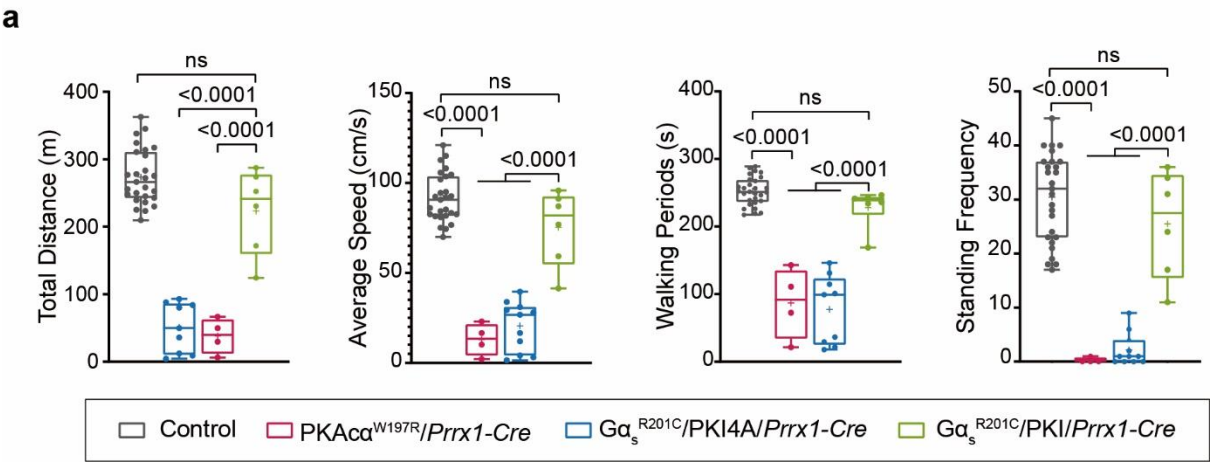

Supplementary Fig. 1. Locomotor activity analyses. (**a**) Locomotor activity analyses of PKA, FD-PKI, FD-PKI4A, and control mice, including measurements of total distance, average speed, walking periods, and standing frequency after Dox administration ($n \geq 6$, one-way ANOVA). The data are presented as box-and-whisker plots, with boxes representing the interquartile range (25th–75th percentiles), the minimum and maximum values reached by bars, the median plotted as a line in the middle, and the mean marked as "+".

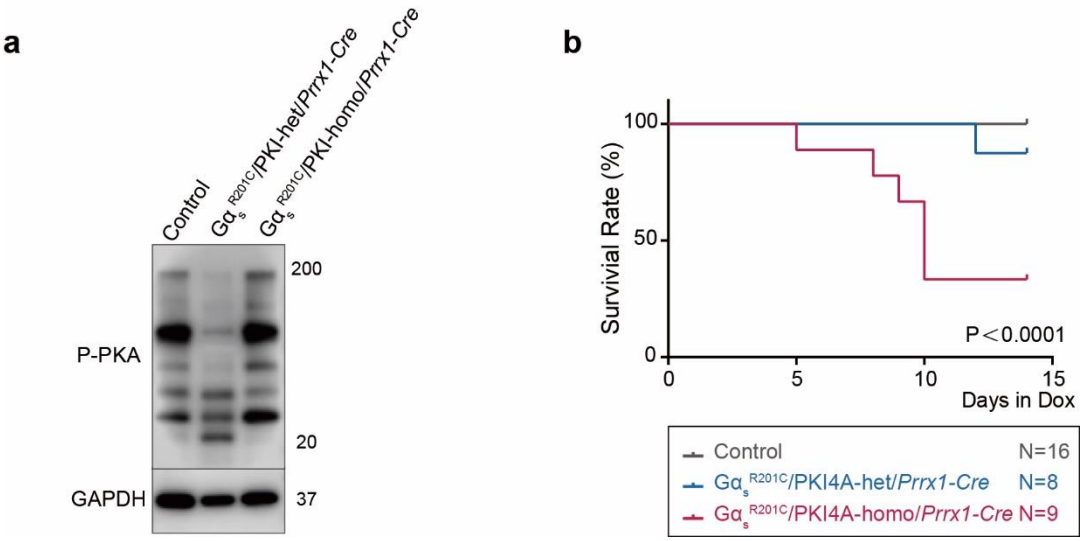

Supplementary Fig. 2. Comparison between heterozygous and homozygous FD-PKI and FD-PKI4A mice. (**a**) Immunoblotting demonstrating reduced phosphorylation levels of PKA in heterozygous FD-PKI mice (Tet-Gα_s^{R201C}/PKI-het/*Prrx1-Cre*), with no suppression observed in homozygous FD-PKI mice (Tet-Gα_s^{R201C}/PKI-homo/*Prrx1-Cre*). (**b**) Kaplan–Meier survival curve comparing heterozygous FD-PKI4A mice (Tet-Gα_s^{R201C}/PKI4A-het/*Prrx1-Cre*, n = 8), homozygous FD-PKI4A mice (Tet-Gα_s^{R201C}/PKI4A-homo/*Prrx1-Cre*, n = 9), and control mice (n = 16), showing a significantly lower survival rate in homozygous FD-PKI4A mice (33.3%) than in heterozygous FD-PKI4A mice (87.5%).

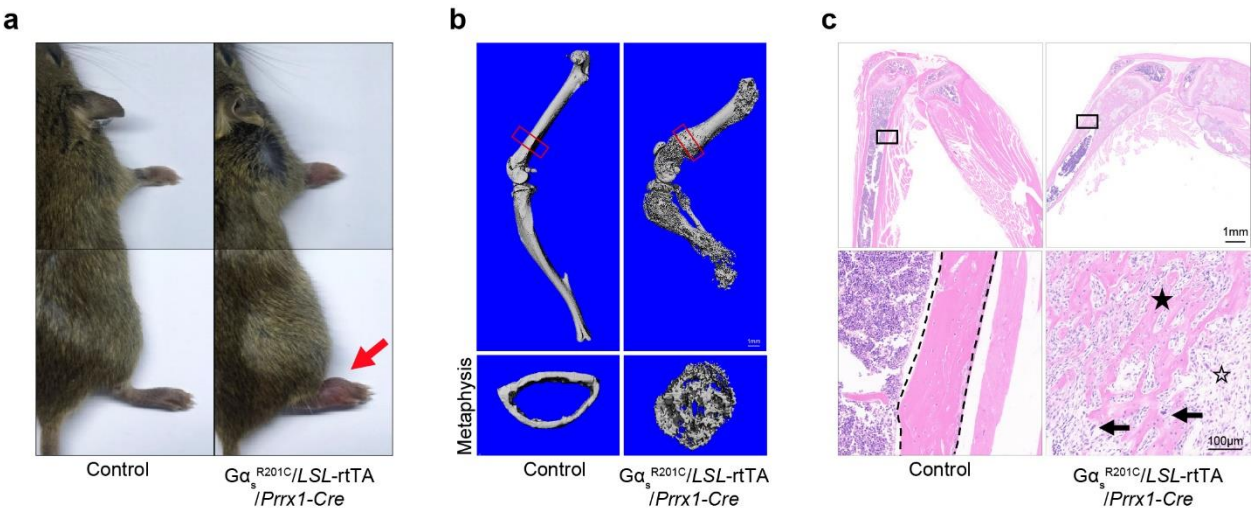

Supplementary Fig. 3. Phenotypic characteristics of FD mice. (**a**) Representative images showing swollen limbs (red arrow) in the Tet-Gα_s^{R201C}/LSL-rtTA/*Prrx1-Cre* mice (FD mice) compared with the control mice. (**b**) Representative images of three-dimensional reconstruction of limb bones from FD mice revealed bone deformity, with expansile lesions observed in cross sections of the metaphysis ROI. (**c**) H&E staining showing typical FD-like histopathological features in FD mice, including irregularly shaped, undermineralized woven bone (black star) lacking osteoblast rimming and embedded within a fibrocellular matrix (white star). Multinucleated osteoclasts (black arrows) were evident on the surfaces of woven bone in FD mice.

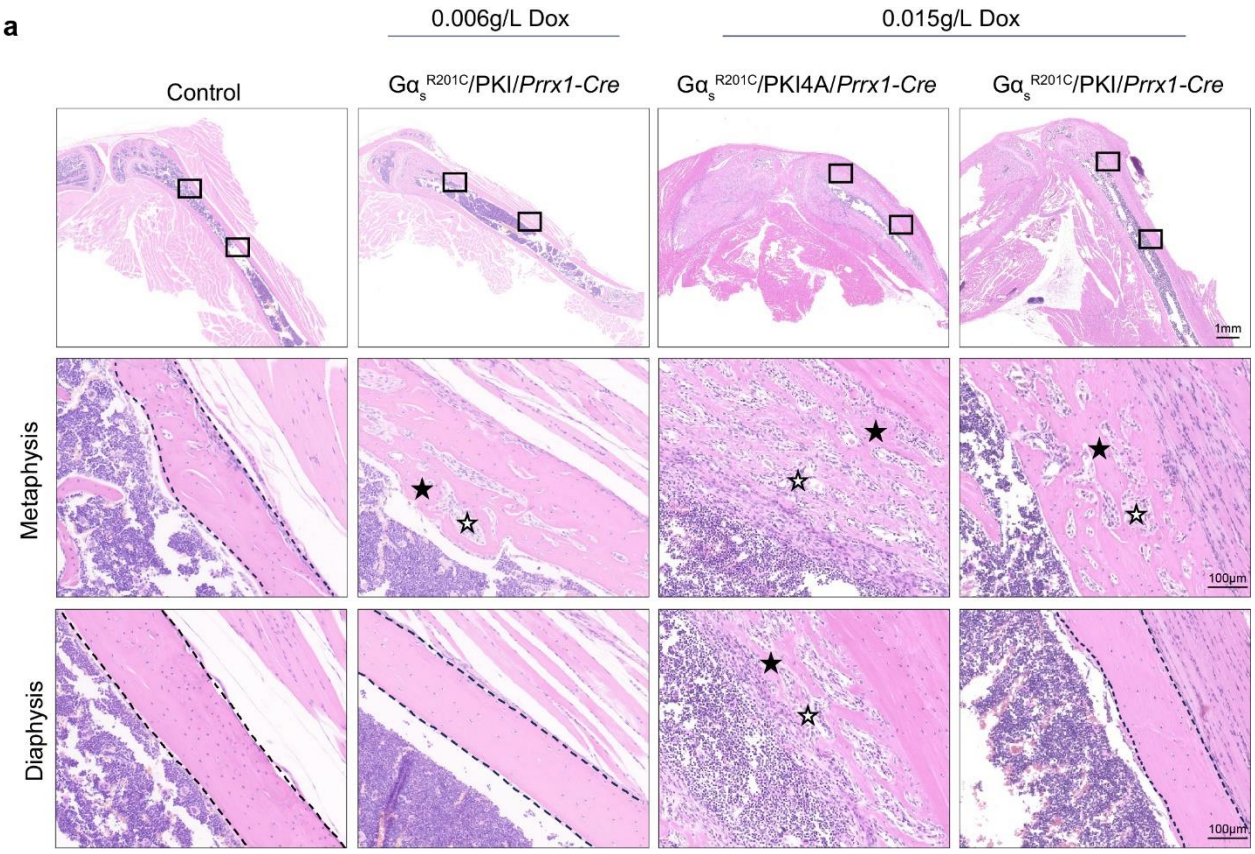

Supplementary Fig. 4. Restricted FD-like lesions in FD-PKI mice. (**a**) H&E staining showing limited FD-like lesions in FD-PKI mice. With a dosing regimen of 0.006 g/L Dox for 2 weeks, only 3 out of 15 FD-PKI mice developed limited FD-like lesions. As the Dox dose increased to 0.015 g/L, the extent of FD-like lesions in FD-PKI mice expanded, accordingly; however, the lesion areas remained significantly smaller than those observed in FD-PKI4A mice under the same induction conditions. These FD-like lesions, characterized by irregularly shaped, undermineralized woven bone (black star) lacking osteoblast rimming and embedded in a fibrocellular matrix (white star), were localized to the metaphysis and did not extend into the bone marrow cavity.

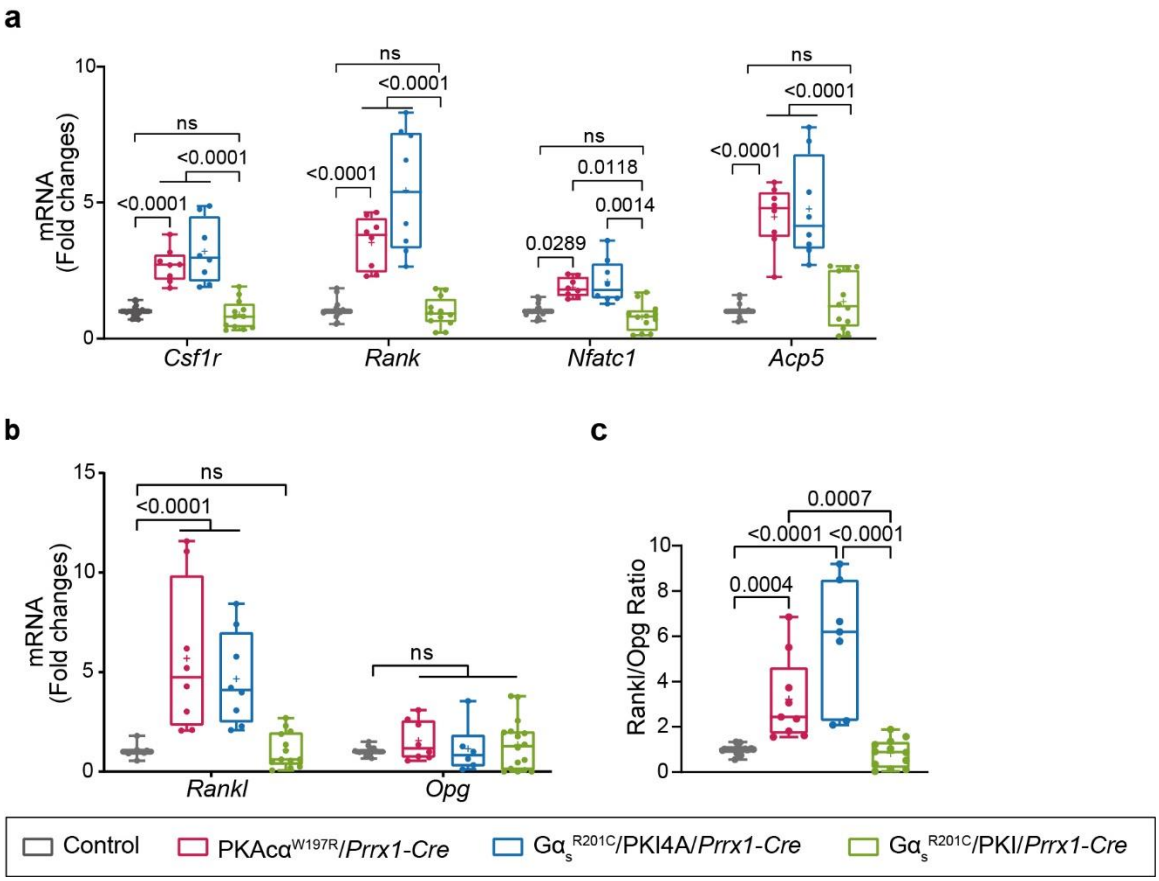

Supplementary Fig. 5. Changes of osteoclast markers and Rankl signaling following PKA modulation. (**a**) qPCR analyses showing osteoclast markers expression levels in bone tissue (n ≥ 6, two-way ANOVA). (**b**) qPCR analyses showing *Rankl* and *Opg* mRNA expression levels in the bone tissue (n ≥ 5, one-way ANOVA). (**c**) qPCR analysis of the Rankl/Opg ratio in bone tissue (n ≥ 5, one-way ANOVA). The data are presented as box-and-whisker plots, with boxes representing the interquartile range (25th–75th percentiles), the minimum and maximum values reached by bars, the median plotted as a line in the middle, and the mean marked as "+".

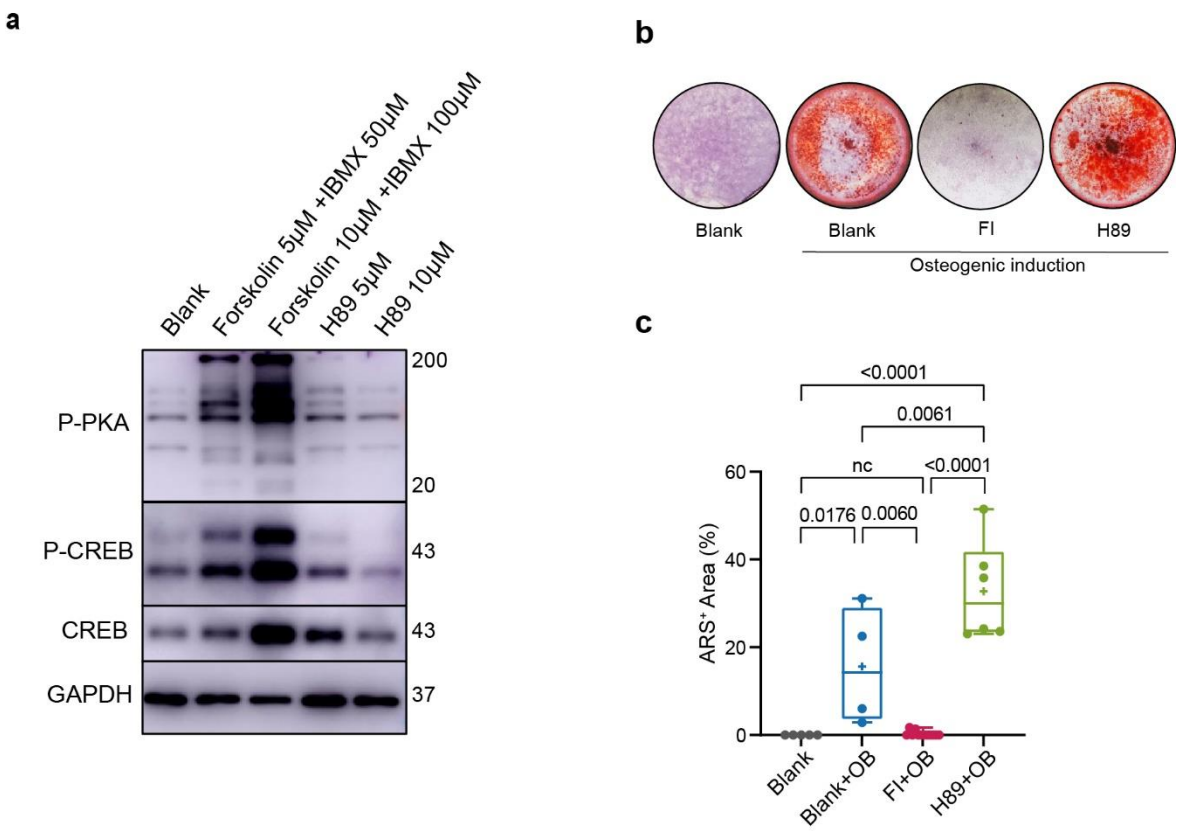

Supplementary Fig. 6. PKA regulates osteoblast differentiation *in vitro*. (**a**) Immunoblotting revealed that phosphorylated PKA and phosphorylated CREB levels in MC3T3-E1-14 cells increased following treatment with forskolin and 3-isobutyl-1-methylxanthine (FI) and decreased with the addition of the PKA inhibitor H89. (**b**) Representative images of alizarin red staining (ARS) and (**c**) quantification of the ARS+ area demonstrated that upregulation of PKA suppressed calcium nodule formation, whereas downregulation of PKA promoted calcium nodule formation. The data are presented as box-and-whisker plots, with boxes representing the interquartile range (25th–75th percentiles), the minimum and maximum values reached by bars, the median plotted as a line in the middle, and the mean marked as "+".